Organic Geochemistry 151 (2021) 104165

Contents lists available at ScienceDirect

Organic Geochemistry

journal homepage: www.elsevier.com/locate/orggeochem

Multi-proxy approach involving ultrahigh resolution mass spectrometry and self-organising maps to investigate the origin and quality of sedimentary organic matter across a subtropical reservoir

Erik Sartori Jeunon Gontijo [a,b], Peter Herzsprung [a], Oliver J. Lechtenfeld [c], Carolina de Castro Bueno [b], Johannes A.C. Barth [d], André H. Rosa [b,*], Kurt Friese [a]

[a] Department of Lake Research, Helmholtz Centre for Environmental Research – UFZ, Brueckstr. 3a, 39114 Magdeburg, Germany
[b] Institute of Science and Technology, São Paulo State University (UNESP), Av. Três de Março, 511, Alto da Boa Vista – CEP: 18087-180, Sorocaba, SP, Brazil
[c] Department of Analytical Chemistry and ProVIS – Centre for Chemical Microscopy, Helmholtz Centre for Environmental Research – UFZ, Permoserstr. 15, 04318 Leipzig, Germany
[d] Department of Geography and Geosciences, GeoZentrum Nordbayern, Friedrich-Alexander University Erlangen–Nürnberg (FAU), Universitätsstraße 40, 91054 Erlangen, Germany

ARTICLE INFO

Article history:
Received 12 July 2020
Received in revised form 14 November 2020
Accepted 19 November 2020
Available online 25 November 2020

Keywords:
Kohonen neural network
^{13}C NMR
FT-ICR-MS
Stable isotopes
Humic substances
Source discrimination

ABSTRACT

Humic substances (HS) in sediments play an important role in carbon and nutrient biogeochemical cycles and fate of contaminants in the environment. However, information regarding HS quality and transformations that may affect their behaviour in reservoirs is still limited. The aim of this investigation was to track sources and changes in sedimentary HS across a subtropical reservoir, connecting them to in-lake processes and land-use influences. Surface sediments were collected at seven sampling sites in Itupararanga Reservoir (Brazil). Humic (HA) and fulvic (FA) acids (components of HS) were extracted from the sediment samples followed by in-depth characterisation via UV/VIS, fluorescence spectroscopy, elemental (C, N) and isotopic analysis (δ^{13}C, δ^{15}N), nuclear magnetic resonance (^{13}C NMR) and Fourier-transform ion cyclotron resonance mass spectrometry (FT-ICR-MS). All data were analysed by self-organising maps. The results showed that samples from the upstream part of the reservoir were older and more decomposed. They likely originated from C3 land-plants (δ^{13}C varied from −26.3‰ to −22.4‰), having more aromatic, oxygen-poor (O/C < 0.5) and unsaturated compounds (H/C < 1.1). In contrast, near-dam samples were younger and had larger contributions of autochthonous material. This was confirmed by oxygen-rich (O/C > 0.5) and partly more unsaturated compounds for FA as well as oxygen-poor and saturated compounds with H/C > 1.1 for HA. Self-organising maps pointed out these differences between upstream and dam areas and indicated that agriculture lands were related to microbially-derived HS. Changes in HS composition revealed that internal reservoir processes may have influenced HS quality across the reservoir.

1. Introduction

Sediments in lakes and reservoirs store a substantial amount of organic matter (OM) and play an important role in the carbon cycle (Chen and Hur, 2015; Guillemette et al., 2017). This OM records processes and conditions from their surrounding catchments and its characterisation provides valuable information about sources and sinks of organic carbon (Torres et al., 2012).

A significant amount of OM in sediments is composed of humic substances (HS) (Chen and Hur, 2015). They are a mixture of organic acids of different molecular sizes with complex structures and mostly derive from decomposition of plants and animal biomass (Raposo et al., 2016). HS can be divided according to their solubility at different pH ranges in fulvic acids (FA, soluble at all pH), humic acids (HA, insoluble at pH below 2) and humin (insoluble at all pH). These substances are also responsible to store refractory organic carbon in sediments and complex to organic pollutants, nutrients, and trace metals, changing their mobility and bioavailability (Nguyen, 1999; Elkins and Nelson, 2002; Li et al., 2018).

The composition and quality of HS depend on their source, which can be allochthonous or autochthonous (Hur et al., 2014; Derrien et al., 2018). While allochthonous material is composed predominantly of lignin and aromatic structures derived from surrounding soils, trees and grasses, autochthonous material is produced from in-lake processes including leachates of dead

* Corresponding author.
E-mail address: andre.rosa@unesp.br (A.H. Rosa).

https://doi.org/10.1016/j.orggeochem.2020.104165
0146-6380/

organisms, macrophytes and phytoplankton. The latter has a more aliphatic character with higher amounts of H and N in its molecules (McDonald et al., 2004; Derrien et al., 2017). The relative contribution of these two sources at each location depends on local and seasonal patterns and can affect OM quality and reactivity (Guillemette et al., 2017). Therefore, investigations of composition and structures of HS can help to understand sources and processes taking place in sediments (e.g. loss of aromatic compounds derived from Fe reduction) (Lovley et al., 1989; Roden et al., 2010; Kulkarni et al., 2018) and their influence on water quality, besides their role on carbon and nutrient cycling (de la Rosa et al., 2011).

Due to the complex characteristics of HS, a combination of several techniques is required to study their composition and structure. Each technique provides complementary pieces of information about the source, structure, and reactivity of HS (de la Rosa et al., 2011). A broad range of methods can be used for HS characterisation, which include elemental composition, fluorescence spectroscopy, UV/VIS absorption, nuclear magnetic resonance (NMR), stable isotopes and recently Fourier transform ion cyclotron resonance mass spectrometry (FT-ICR-MS) (Hertkorn et al., 2013; Minor et al., 2014; Melendez-Perez et al., 2016; Herzsprung et al., 2017b). FT-ICR-MS combined with electrospray ionisation (ESI) provides detailed information on the molecular composition of HS typically resolving several thousand different molecular masses in HS. It enables molecular formula assignment to constituents of complex mixtures including non-fluorescent compounds of OM (Koch and Dittmar, 2006; Zherebker et al., 2016; Derrien et al., 2018).

The acquisition of large volumes of data by several techniques requires tools that simplify the interpretation of the results with synoptic visualisation capabilities. Artificial neural networks such as self-organising maps meet these needs because they can cluster and recognise patterns in complex data sets. This technique has been successfully used for discriminating organic matter fluorescence components (Ejarque-Gonzalez and Butturini, 2014), the evolution of fluorescent dissolved organic matter in treatment plants (Yang et al., 2019), water quality and identification of specific biogeochemical processes in waters (desorption of Fe, Mn and nutrients from sediments and algal growth) (Çinar and Merdun, 2009; Melo et al., 2019).

Past investigations have combined different techniques (e.g. ^{13}-C NMR, fluorescence, pyrolysis gas chromatography–mass spectrometry and stable isotopes) to study OM from sediments (Wolfe et al., 2002; de la Rosa et al., 2011; Guillemette et al., 2017; Li et al., 2018). However, only a few of them included FT-ICR-MS to characterise FA and HA and to track their sources (Dadi et al., 2017; Valle et al., 2018). Therefore, further studies about the potential of FT-ICR-MS to discriminate the sources of sedimentary OM are promising for getting a better picture of local and global carbon cycles (Derrien et al., 2018).

The main purpose of this study is to track sources, molecular composition and structural information of sedimentary FA and HA along a tropical reservoir with absorbance, fluorescence spectroscopy, stable isotopes and to combine them with ^{13}C NMR, FT-ICR-MS and self-organising maps. Possible changes in the HS were then investigated with the aim to identify in-lake processes and land-use influences around the reservoir. A novel focus on FT-ICR-MS intended to discriminate molecular changes in sedimentary HS and the combination of this information with self-organising maps is promising to provide integral information of all data collected. This multi-proxy study was promising to yield new information about refractory organic matter in sediments to identify possible biogeochemical processes including oxygen consumption and redox reactions. These processes may also influence the water quality of reservoirs that are important for drinking and irrigation (Meyers and Ishiwatari, 1993).

2. Material and methods

2.1. Study site and sampling

Itupararanga Reservoir is located in Sorocaba River catchment in the state of São Paulo, southeast of Brazil, with a storage volume of 286 million m^3, a catchment area of about 934 km^2 and a reservoir area of 19 km^2. Its length is 26 km and maximum and average depths are 21 and 7.8 m, respectively (Ribeiro et al., 2014; Frascareli et al., 2018). The average water residence time in the reservoir is 250 days (Frascareli et al., 2015; Rodrigues et al., 2019). It was constructed in 1912 originally for hydroelectricity generation and currently serves multiple purposes including irrigation and drinking water supply for approximately one million people (Pedrazzi et al., 2013). The reservoir is seasonally stratified in the warm season (October to March), when dissolved oxygen in its bottom waters can decrease to values around 1 mg L^{-1} (Melo et al., 2019).

Surface sediment samples (approx. 10 cm thickness) were collected in December 2016 at seven sampling locations (P1 - P7, Fig. 1) with a grab sampler. These sampling locations were selected in previous investigations (Rosa et al., 2015; Melo et al., 2019) based on land use, horizontal compartmentalisation of the reservoir and influence of inflows. The water depth and additional information about each sampling site are available in Appendix A (Table A.1). All collected samples were freeze-dried in the laboratory for HS extraction. The particle size distribution of the sediments was analysed by a laser-diffraction system (CILAS 1190; Quantachrome, Germany).

2.2. Land use

Land use data from the 1-km shoreline buffer zone around the reservoir and downstream portions of its main tributaries helped to study sources of HS in surface sediments. This buffer zone may stronger reflect the effects of the land use in the reservoir than regional effects on a catchment scale (Shen et al., 2015; Zorzal-Almeida et al., 2018). Areas that covered the length from each sampling site to 8 km upstream were attributed for each site inside this buffer zone (Fig. A.1, appendix A). Moreover, the land use on the entire catchment was also considered in the results.

The catchment boundaries of the reservoir were outlined using Shuttle Radar Topography Mission (SRTM) data (1:250.000) downloaded from Embrapa (de Miranda, 2005). Cloud free Landsat 8 images (219/76, 12th September 2017 and 30 m resolution) acquired from the webpage of EarthExplorer (https://earthexplorer.usgs.gov/, accessed in June 2018) and RapidEye images (5 m spatial resolution from 17th July and 30th August 2014) were used for land cover classification. Five different land use types (agriculture, forest, pasture, silviculture and urban) were defined and their proportions were calculated for the whole catchment as well as the areas defined for each sampling site in the buffer zone. All delineations and calculations were carried out in the software ArcGis 10.5 (ESRI, USA).

2.3. Humic and fulvic acid extraction

HA and FA were extracted from sediments based on the International Humic Substances Society (IHSS) method (Swift, 1996). Briefly, the extractions were performed using 0.1 mol L^{-1} HCl and NaOH solutions at a ratio of 1 g of sample to 10 mL of solution. The alkaline step was carried out under N_2 atmosphere for 4 h. HA were dialysed against ultrapure water (dialysis tubing cut-off was 3500 Da) to reduce their salt contents. FA were passed through a

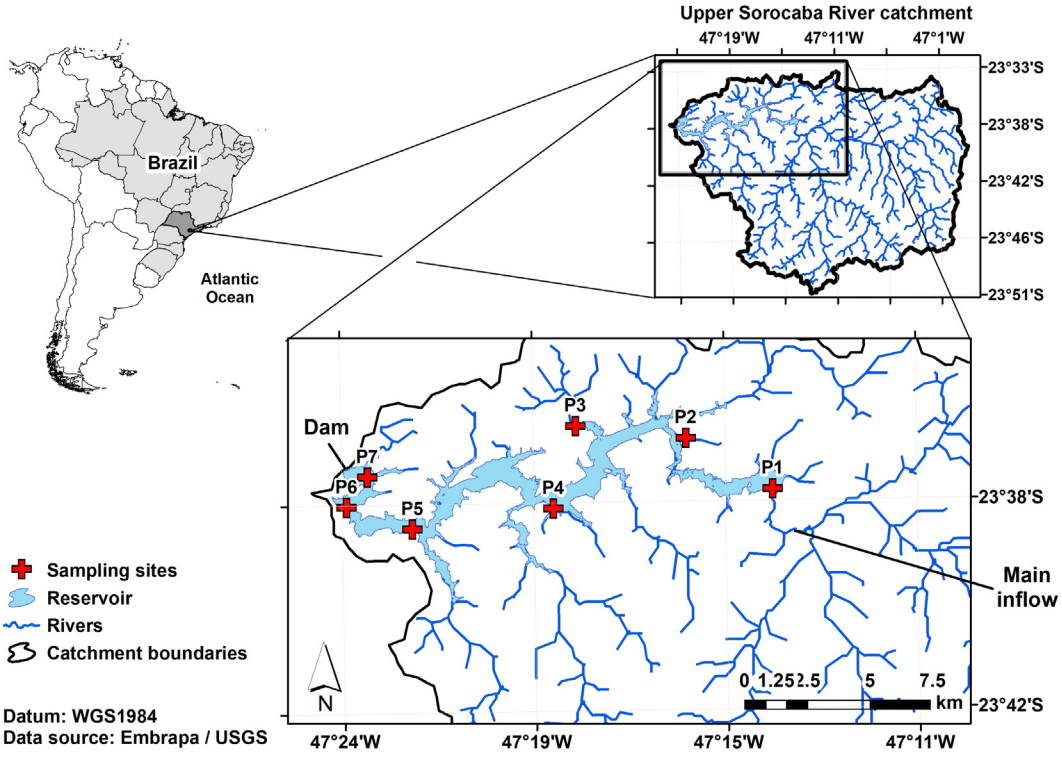

Fig. 1. Location of the seven sampling sites (represented by crosses) in the Itupararanga Reservoir.

column of Supelite™ DAX-8 resin. Both FA and HA extracts were dried at 45 °C for further analyses.

The dry samples were weighed to determine the percentage of extracted HA and FA per sampling station. The organic and inorganic contents of the dried and ground sediments were determined by combustion (loss on ignition) at 550 °C in a muffle oven for 4 h (Dean, 1974). The organic content was calculated by the difference between the raw dried sample (105 °C) and the remaining residue after the heating (550 °C).

2.4. Optical spectroscopic measurements

Absorbance spectra (240–600 nm) and fluorescence data from FA and HA were recorded simultaneously in a 1 cm quartz cuvette using a spectrofluorometer Aqualog® (HORIBA Jobin Yvon, Edison, New Jersey). The fluorescence intensity was measured during emission scans (240 to 600 nm, every 3.27 nm, 8 pixels) at set excitation wavelengths in 3 nm increments from 240 nm to 600 nm. The bandpass used for excitation and emission wavelengths was 5 nm and the integration time of 0.25 s was used. The method is detailed described by Herzsprung et al. (2017a).

The fluorescence index (FI), a proxy for distinguish between microbially and terrestrially derived OM, was calculated by the ratio of fluorescence intensity at emission wavelength at 470 to 520 nm at an excitation wavelength of 370 nm (McKnight et al., 2001). The humification index (HIX), a proxy related to the degree of humification of OM, was calculated as the area under the emission spectra between 435 and 480 nm divided the sum of peak areas between 300 and 345 nm (Ohno, 2002). The freshness index (β/α), an indicator of recently produced OM, was calculated dividing the emission intensity at 380 nm to the maximum emission intensity between 420 and 430 nm at excitation 310 nm (Parlanti et al., 2000; Hansen et al., 2016). The proxy for the molecular size of HA and FA was calculated through the E2:E3 ratio, which is calculated dividing the absorbance at 254 nm by the absorbance at 365 nm (Helms et al., 2008).

2.5. Distribution of carbon through ultrafiltration

The distribution of organic carbon was assessed through ultrafiltration using a Stirred Ultrafiltration Cell (SUC) system (Model 8200, Millipore™). Solutions from HA and FA dried extracts were prepared (9.6 ± 1.0 mg L^{-1} of total organic carbon, TOC) and filtered sequentially in regenerated cellulose membranes of 100, 30, 10, 5 and 1 kDa, which resulted in 6 (F1 - F6) different fractions (F1 > 100 kDa; 30 < F2 < 100 kDa; 10 < F3 < 30 kDa; 5 < F4 < 10 kDa; 1 < F5 < 5 kDa; F6 < 1 kDa), whose volumes were adjusted to ca. 40 mL (except F6). The exact initial and filtered volumes were measured and the organic carbon content (OCC) of each fraction was measured using a total carbon analyser (DIMATOC® 2000, Dimatec Analysentechnik GmbH, Germany) for calculation of the organic carbon balance.

2.6. Elemental analysis

The elemental composition (C, N) of the dried HA and FA was analysed using an Elemental Combustion System (Costech Instruments). The elemental composition of the samples was used for calculation of the C:N ratio which is generally used as a proxy to distinguish material originated from algae (C:N between 4 and 10) and land-plants (C:N ≥ 20) (Meyers, 1994). The elemental composition of the raw sediments was also determined using a CN analyser (DIMATOC 2000, DIMATEC Analysentechnik GmbH, Germany); reproducibility and accuracy was better than 3%.

2.7. ^{13}C nuclear magnetic resonance (^{13}C NMR)

Solid-state nuclear magnetic resonance on ^{13}C (^{13}C NMR) spectroscopy of HA and FA provides direct information about the rela-

tive amounts of different carbon structural units of humic molecules (Conte et al., 2002). The solid-state ^{13}C NMR spectra were recorded on a Bruker AV 300 WB operating at a frequency of 75.47 MHz. Magic angle spinning (MAS) was performed at 15 kHz with zirconium dioxide rotors (diameter 4 mm). The cross polarisation (CP) contact time was 2000 ms and the number of accumulated scans was 10,000. The ^{13}C NMR spectra were subdivided into six chemical shift regions according to the chemical type of ^{13}C carbon following Knicker and Lüdemann (1995): alkyl C (0–45 ppm), N-alkyl/methoxyl C (45–60 ppm), O-alkyl C (60–110 ppm), aromatic C (110–160 ppm), carboxyl/amide C (160–185 ppm) and carbonyl C (185–220 ppm). The aliphaticity and aromaticity were estimated from the calculation of the relative area (%) under the spectra from 0 to 110 and 110 to 160 ppm, respectively (Rodríguez-Murillo et al., 2011).

2.8. Stable isotope analysis ($\delta^{13}C$ and $\delta^{15}N$)

The analysis of stable isotopes ($\delta^{13}C$ and $\delta^{15}N$) of FA, HA and raw sediments was performed using a Delta V Plus Isotope Ratio MS (Thermo Scientific) coupled with an elemental analyser (Costech Instruments). All isotope ratios were expressed in a per mille (‰) notation and calculated according to the Eq. (1) (Craig, 1957):

$$\delta^{13}C \text{ or } \delta^{15}N = \left(\left(R_{sample}/R_{reference}\right) - 1\right) \times 1000 \quad (1)$$

where R is the ratio of the heavy to the light carbon isotopes and the references (standards) were the Vienna Pee Dee Belemnite and atmospheric N_2 for C and N, respectively. All results were corrected to instrumental drift and linearity.

2.9. High-resolution FT-ICR-MS analysis

2.9.1. Solid-phase extraction (SPE)

HA and FA extracts were re-dissolved in ultra-pure water (MQW, Integral 5, Merck, Darmstadt, Germany) and extracted via solid-phase extraction (SPE) in order to reduce remaining salts in the samples for subsequent direct ESI-MS (Dittmar et al., 2008; Raeke et al., 2016). For SPE, 50 mg styrene-divinyl-polymer type sorbents (Bond Elut PPL, Agilent Technologies, Santa Clara, CA, United States) were loaded with 175 ± 20 and 560 ± 60 μg of carbon for FA and HA, respectively. The SPE-OM was eluted with 1 mL methanol (Biosolve, Valkenswaard, Netherlands), diluted to 20 ppm and mixed 1:1 (v/v) with ultrapure water (Milli-Q Integral 5, Merck, Darmstadt, Germany) immediately prior FT-ICR-MS analysis. Carbon-based extraction efficiency was approx. 61% for the FA and 6% for the HA samples.

2.9.2. FT-ICR-MS measurement

An FT-ICR mass spectrometer equipped with a dynamically harmonised analyser cell (solariX XR, Bruker Daltonics Inc., Billerica, MA, USA) and a 12T refrigerated actively shielded superconducting magnet (Bruker Biospin, Wissembourg, France) instrument located at the ProVIS Centre for Chemical Microscopy within the Helmholtz Centre for Environmental Research was used in ESI negative ionisation mode (capillary voltage: 4.2 kV). Extracts were analysed in random order with an autosampler (infusion rate: 10 μL min^{-1}). For each spectrum, 256 scans (ion accumulation time: 40 ms for FA and 30 ms for HA) were co-added in the mass range 150-1000 m/z with a 4 MWord time domain (resolution at m/z 400: ca. 483,000). Mass spectra were internally calibrated with a list of peaks (250-640 m/z, n > 125) commonly present in terrestrial dissolved OM and the mass accuracy after internal calibration was better than 0.18 ppm (n = 14). Peaks were considered if the signal/noise (S/N) ratio was greater than four. Raw spectra were processed with Compass DataAnalysis 5.0 (Bruker Daltonics Inc., Billerica, MA, USA).

2.9.3. Data processing

Molecular formulas were assigned to peaks in the range 0-750 m/z allowing for elemental compositions $^{12}C_{1\text{-}60}$, $^{13}C_{0\text{-}1}$, $^{1}H_{0\text{-}122}$, $^{16}O_{0\text{-}40}$, $^{14}N_{0\text{-}4}$, $^{32}S_{0\text{-}1}$, and $^{34}S_{0\text{-}1}$ with an error range of ±0.39 ppm. Only formulas with $0 \leq DBE \leq 25$ and $-10 \leq DBE\text{-}O \leq +10$ (DBE (double bound equivalent) = 1 + 1/2 (2C − H + N)) were considered for further data evaluation (Koch et al., 2014; Herzsprung et al., 2016). Isotopologue formulas (^{13}C, ^{34}S) were used for quality control but removed from the final data set as they represent duplicate chemical information. Molecular formulas present in full process blanks (n = 2) were removed from the entire data set, if their peak abundance was at least once higher than the lowest intensity within the 14 samples. Relative peak intensities (RI) were calculated based on the summed intensities of all assigned peaks in each sample (Flerus et al., 2012). In addition, intensity ranks were calculated for each of the 14 samples as described by Herzsprung et al. (2012), tables A.2-A.6 (Appendix A). The average nominal oxidation state of carbon (NOSC), DBE and modified aromaticity index (AI_{mod}) were calculated from the peak masses and molecular formulas, according to Koch and Dittmar (2006) and LaRowe and Van Cappellen (2011) (cf. Appendix A).

To compare the OM quality, hierarchical cluster analysis (HCA, using Euclidian distance and Wards minimum variance clustering method) was performed for all 14 samples and FA and HA sets separately. The intensity ranks which were separately calculated for FA and HA were further used for calculation of inter sample ranks as described by Herzsprung et al. (2012) and Herzsprung et al. (2017a). The inter sample ranks were used in van Krevelen diagrams.

2.10. Self-organising maps

The data set used in the analysis (example in Table A.7, Appendix A) included all FA and HA samples and 24 variables that contain all results of chemical characterisation (i.e. absorbance and fluorescence indices, $\delta^{13}C$ and $\delta^{15}N$ isotopic composition, C:N ratio, summed relative intensities of CHO, CHNO, CHOS and CHNOS molecular formulas obtained via FT-ICR-MS and percentages of integrated areas obtained via ^{13}C NMR) and proportions of land use areas.

The structure of the self-organising maps was two-dimensional and organised in hexagonal grids. The data set was initially normalised via z-score transformation to convert the variables to a common scale with mean zero and standard deviation one. This avoids the dominance of a variable or group of variables (Asan and Ercan, 2012). The batch training algorithm was used for training the self-organising maps. Different architectures (4×4 to 7×7) were tested for setting the number of output nodes (neurons) in the self-organising maps. The selected architecture should have an optimal number of neurons. This is because too high or too low numbers would result in samples clustered together or too far apart. This, in turn, would reduce the possibility to extract information (Garcia et al., 2007).

The analysis was performed in MatLab version 2017b (MathWorks, Natick, MA) using the SOM toolbox 2.1 (freeware, available online on the website http://research.ics.aalto.fi/software/somtoolbox/, accessed in May 2018) (Alhoniemi et al., 2000). More details can be found in Appendix A. Principal component analysis (PCA) of the data was carried out to highlight the advantages of using self-organising maps.

3. Results

3.1. Particle size and organic matter content

The particle size distribution of the samples showed higher proportion of sand (particle size between 63 and 2000 μm) in the surface sediments at P1 (59.5%). This sand proportion decreased within the samples towards the dam (13.6% at P7). In contrast, silt (particle size between 2 and 63 μm) and clay (particle size < 2 μm) proportion increased within samples towards the dam (Fig. A.2, Appendix A). The OM content in the surface sediments analysed varied between 4.1 (at P1) to 17.2% weight (at P5). The lowest contents were recorded in the upstream areas of the reservoir, especially from P1 to P3 (Table A.8, Appendix A). The data showed that the sedimentary OM content is related to the sediment texture (higher clay and silt proportions suggest higher amounts of OM). HA made up most of the HS extracted from these sediments (Table A.8, Appendix A).

3.2. Absorbance, fluorescence and isotopic composition

Fig. 2 presents the isotopic composition, absorbance and fluorescence indices of sedimentary HA and FA from the reservoir. The E2:E3 ratios serve as proxies for molecular size and indicated that HA presented relatively constant average molecular sizes (E2:E3 between 2.54 ± 0.01 at P5 and 2.75 ± 0.01 at P1) along the reservoir.

In contrast, larger variations of E2:E3 were observed among FA samples, from 4.60 ± 0.05 at P2 to 6.31 ± 0.04 at P5. These variations could not be observed in the organic carbon distribution of the extracts (Fig. A.3, Appendix A). The predominant molecular fraction (obtained by ultrafiltration, Section 2.5) of FA from all samples was F4 (5 < F4 < 10 kDa; 29-38% of the organic carbon content). On the other hand, a larger molecular fraction size (F1 > 100 kDa; 62-99% of the organic carbon content) was the predominant fraction in the HA samples. This was also expressed by their much lower E2:E3 ratios when compared to the FA samples.

Regarding fluorescence indices and elemental composition, our results indicated that sampling sites in upstream reaches of the reservoir (P1 - P3) had lower β/α values for FA and HA than samples from the dam area (P5 - P7). The FI also presented similar trends of increasing values towards the dam area.

The sampling locations P3, P6 and P7 had the lowest C:N values. In contrast, samples from upstream reaches (P1 - P2) the had the highest ones. All samples presented high and relatively constant HIX values (ca. 0.8 to 0.9) along the reservoir. This implies a similar level of diagenesis and a high degree of humification, especially for FA (Hansen et al., 2016).

The FA and HA from the reservoir were depleted in ^{13}C with values ranging from −26.3‰ to −22.4‰). This suggests that the samples were derived predominantly from C3 plants. Fig. 2f shows only small variations of the isotopic composition along the reservoir, except for locations P5 and P6 that were more enriched in ^{13}C and had $\delta^{13}C$ values of up to −22.4‰ at P5 (HA).

Our $\delta^{15}N$ results showed that samples were enriched in ^{15}N with values between +4.5 and +5.8‰. The isotopic composition of organic matter analysed in the raw sediments was similar to the observed in the extracted HS (Table A.8, Appendix A).

3.3. ^{13}C nuclear magnetic resonance (^{13}C NMR)

The integration of ^{13}C NMR spectra (cf. Figs. A.4 and A.5, Appendix A) indicated more pronounced changes among FA samples than HA samples along the reservoir. For instance, samples P6FA and

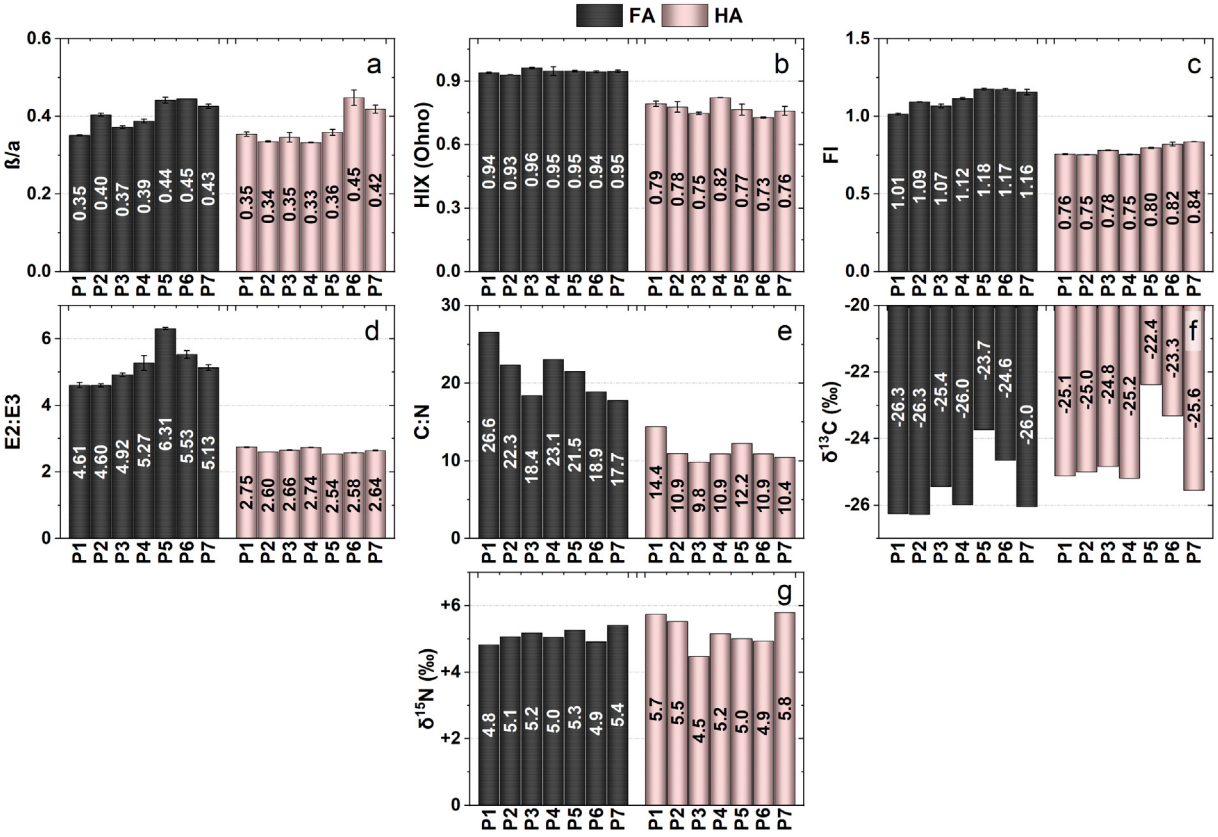

Fig. 2. Freshness index (β/α; a), humification index (HIX; b), fluorescence index (FI; c), E2:E3 ratio (d), C:N ratio (e) and isotopic composition (f and g) of sedimentary fulvic (FA) and humic (HA) acids of the seven sampling sites in Itupararanga Reservoir.

P7FA showed the highest abundance of O-alkyl C (37.1 and 32.6% of the total integrated area, respectively) and the lowest abundance of aromatic C (1.8% of the total integrated area at P7FA). FA samples from the dam area (P5 - P7) had the highest aliphaticity (from 59.4 to 77.3%) as estimated by ^{13}C NMR spectra (Table A.9, Appendix A).

3.4. FT-ICR-MS analysis

Between 4539 and 6135 molecular formulas were assigned to approx. 18,000 mass peaks in the FA samples while 6673-8982 formulas were assigned to 22,500 peaks the HS samples by FT-ICR-MS. CHO formulas contributed most (>40%) to the molecular space of FA samples extracted from P1 to P6 (Table A.10, Appendix A).

In contrast, N-containing formulas (in particular CHNO) were dominant (>40%) for P7FA and all HA samples (P1HA - P7HA). Especially P7FA was different from the other FA samples, because of its higher peak intensities for CHNO molecules (cf. Table A.11, Appendix A). In addition, P7FA was composed of the most oxidised molecules with the highest NOSC (0.201, cf. Table A.12, Appendix A). In contrast, P6HA and P7HA contained the most reduced molecules (NOSC = −0.200 and −0.153, respectively) on average.

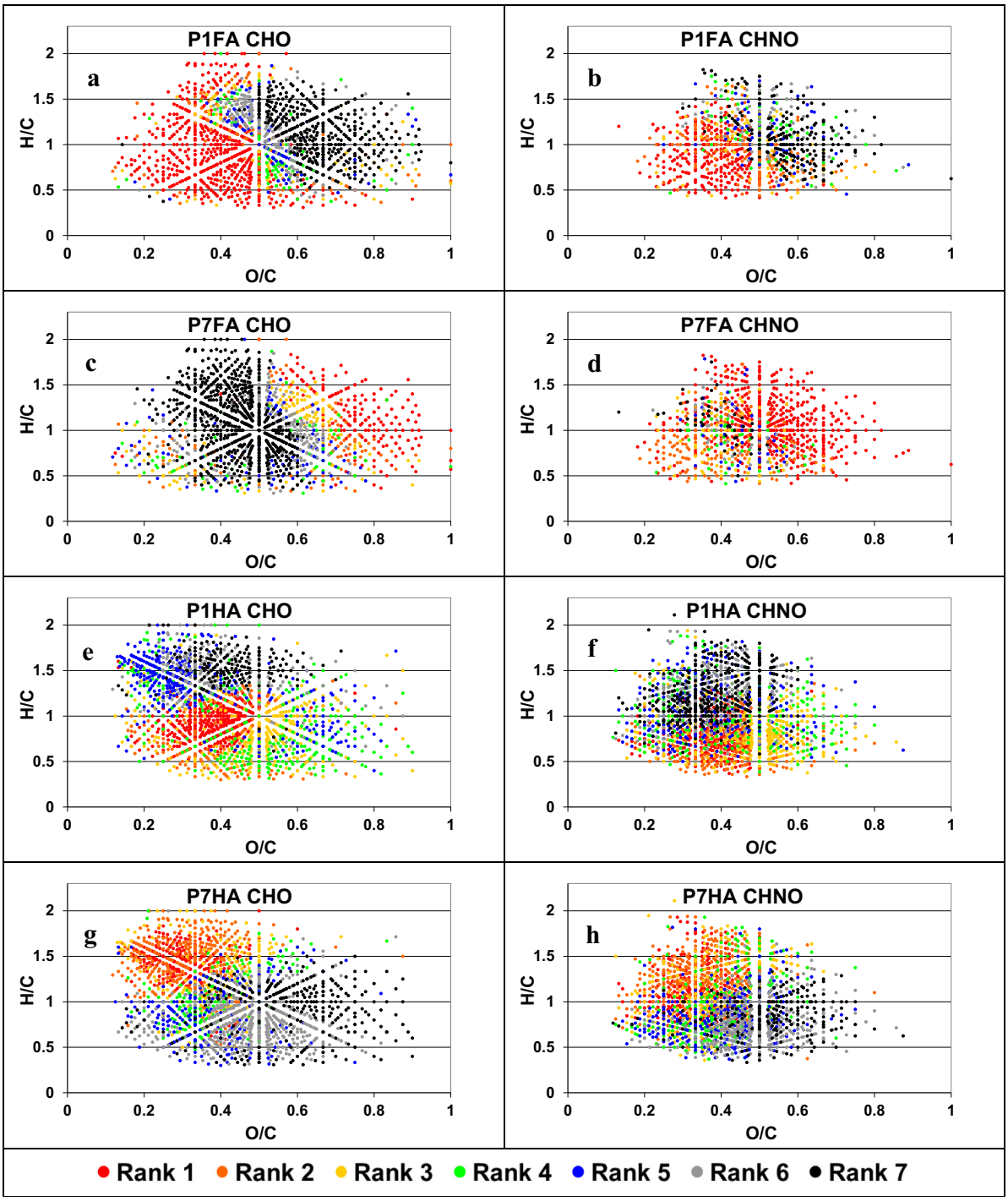

Fig. 3. Van Krevelen diagrams produced from inter sample ranking analysis from humic (HA) and fulvic (FA) acid samples: P1FA (a for CHO and b for CHNO), P7FA (c for CHO and d for CHNO), P1HA (e for CHO and f for CHNO), P7HA (g for CHO and h for CHNO).

In a second step, the OM quality of samples can be distinguished by multivariate statistical means using HCA. Fig. A.6 (Appendix A) shows that FA and HA samples differ considerably from each other when compared to samples P1 to P7 (FA or HA). Due to this discrepancy, we show the OM quality differences for FA samples separately from those of HA samples.

Concerning all formulas that were present in all 7 FA samples, the HCA (Fig. A.7 a, Appendix A) shows that sample P1FA and in particular P7FA are different from all other FA samples and from each other. The strongest similarities were found between P5FA and P6FA and between P2FA and P4FA respectively. Similarities between HA were different from those for FA. P6HA and P7HA samples were similar to each other and both samples were rather different from all other HA samples (Fig. A.7 b).

While the HCA analysis tests if samples are different from each other, the inter sample ranking analysis visualises the difference of chemistry between samples using van Krevelen diagrams. In the following, the chemical differences preferably between P1FA and P7FA and between P1HA and P7HA respectively are described considering the relative high differences found in the HCA.

Fig. 3 shows van Krevelen diagrams produced from inter sample ranking analysis for P1 and P7 (FA and HA) for CHO and CHNO (with the highest relative intensities in all samples) formulas. It shows specific differences in the organic matter quality among FA and HA extracted along the reservoir (see Figs. A.8 and A.9, Appendix A, for diagrams of all samples). Regarding FA and CHO molecules, the upstream sample (P1FA, Fig. 3 a) showed high intensities for oxygen-poor molecules (O/C < 0.5) with exceptions for molecules with 1.1 < H/C < 1.6 and O/C > 0.4 (Fig. 3). The CHNO showed a similar trend for the oxygen-poor molecules except for the more aliphatic ones (H/C > 1.5). The near dam FA (P7FA) CHO showed high intensities for oxygen-rich molecules (O/C > 0.5), whereas the oxygen-poor molecules showed the relative lowest intensities in this sample (Fig. 3 c). A large portion of CHNO seems to be enriched (regarding the accumulation of first and second ranks) in the P7FA sample compared to all other FA samples (Fig. A.8, Appendix A).

The OM quality change between upstream and near dam samples for HA was different from FA samples. Whereas FA changed to more oxygen-rich quality towards the dam, the HA changed to more aliphatic quality. In the P1HA sample, the highest intensities were found to be oxygen-poor and unsaturated molecules (H/C < 1.1). The P7HA sample (Fig. 3 g and h) showed also higher intensities for oxygen-poor molecules, however, in contrast to P1HA it had higher intensities for aliphatic molecules (H/C > 1.1).

In the HA samples the rank distribution of CHNO and CHO were more similar to each other when compared to the FA samples (Fig. A.9, Appendix A). It is remarkable that concerning HA, oxygen-rich molecules showed the most first and second ranks in samples PHA3 and PHA5 and oxygen-poor molecules the most seventh and sixth ranks.

3.5. Self-organising maps

The self-organising maps analysis clustered the samples in five groups (I - V) (Fig. 4 a). The map architecture with 5 × 5 neurons was chosen for self-organising map analysis because it was the most informative and provided the best distribution of samples. The samples grouped in the same or in neighbouring neurons (hexagonal units in Fig. 4) are considered similar to each other according to the input variables. The larger the distance between two neurons in the map, the more different are the samples (da Silva et al., 2008). The maps of variables are presented in Fig. 4 b, where the colour bars beside the maps correspond to the intensi-

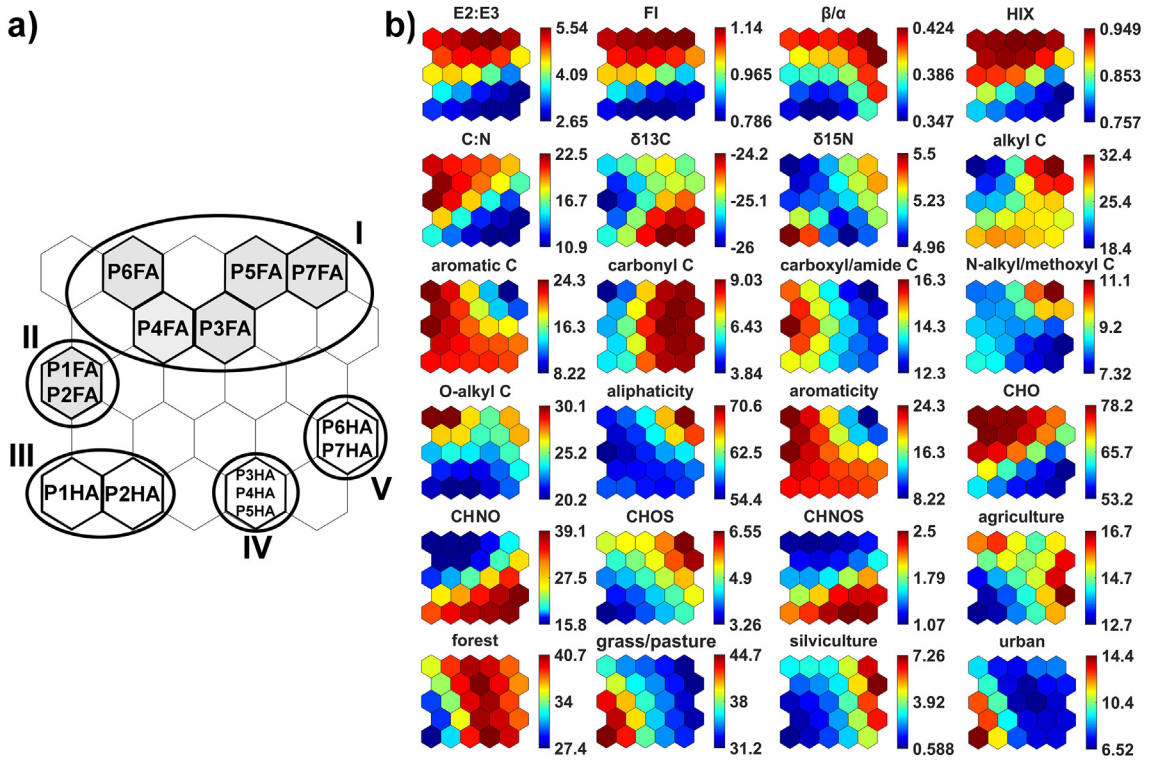

Fig. 4. Self-organising maps for fulvic (FA) and humic (HA) acids samples extracted from surface sediments from Itupararanga reservoir: (a) map of samples; (b) maps of variables (component planes). The grey colour in the neurons (hexagonal units) of the map of samples (a) stands for FA and the white colour neurons with samples represent HA. Samples in the same or neighbouring neurons are considered remarkably similar and were clustered in five distinct groups (I - V). The red and blue colours in the maps of variables indicate high and low intensity for the variables (for interpretation of the references to colour in this figure legend, the reader is referred to the web version of this article).

ties of each variable. Blue and red colours in the maps represent low and high intensities, respectively.

All FA samples are located in the upper part of the map (groups I and II, Fig. 4 a) and all HA samples are located in the bottom (groups III - V) in the map of samples (see these two distinct regions in Fig. 4 a). This supports the fact that the differences between FA and HA were larger than the differences among the sampling sites (P1 - P7) either for FA or HA, as observed in HCA analysis for the complete molecular data set. These larger distinctions can be attributed to the more pronounced intensity of the variables FI, β/α, HIX, E2:E3 and CHO for FA samples in upper groups. This is shown by the red colours in Fig. 4 b at the position of neurons where FA samples are located (i.e. groups I and II). Moreover, FA groups presented lower intensities than HA for CHNO and CHNOS.

Inter-site differences in the reservoir could also be observed in the maps of variables such as aromaticity, carbonyl C, C:N, CHO, FI and β/α. These variables presented higher intensities (Fig. 4 b) either for upstream sites (groups II and III, left side of maps in Fig. 4) or near-dam sites (groups I, IV and V, mostly in the right side of maps in Fig. 4). Samples from groups II and III (i.e. P1 and P2) for instance presented FA and HA with higher intensities for C:N and lower intensities for β/α and FI than samples from near-dam areas (P5 - P7 in groups I, IV and V, Fig. 4 a). This can be observed by comparing the colours of the neurons in FI, C:N and β/α maps, Fig. 4 b, at correspondent positions of the analysed samples shown in Fig. 4 a. These differences indicate OM quality differences between upstream and near-dam locations in the reservoir. Moreover, greater distances in the map are related to larger differences between samples. Samples P4FA and P5FA (group I) for instance are more different from each other than samples P4HA and P5HA (group IV) because the FA samples are farther from each other than the correspondent HA samples which are in the same neuron. This suggests that FA were better for finding inter-site differences since most of their samples were located in different neurons and farther from each other than HA samples. Table A.13 (Appendix A) describes the variables with high intensity in each group from Fig. 4 a.

4. Discussion

4.1. Sedimentary fulvic and humic acids

The differences between FA and HA were dominant when compared to the internal differences among FA samples and HA samples (Fig. A.6). This trend was expected due to sample preparation (extraction procedure) and the typical distinctions between FA and HA. The FA samples for instance presented smaller average molecular size, higher content of oxygen compounds (CHO) and higher C:N ratio than HA. The ^{13}C NMR data showed that the larger oxygen content of FA may be related especially to the greater presence of O-alkyl C compounds. The higher C:N ratio of FA may be attributed to a higher proportion of terrestrial source and preferential microbial utilisation of smaller-sized OM that may contain higher N content prior HS formation (Meyers and Ishiwatari, 1993; Hur and Kim, 2009). In addition, the use of DAX-8 resin in the process of FA extraction may have contributed to increase the C:N ratio of FA by taking away loosely associated N from its structure (See and Bronk, 2005).

Differences between FA and HA can also be visualised in van Krevelen and mass diagrams of contrasting occurrence of molecular formulas in FA and HA samples (Fig. A.10, Appendix A). Many oxygen-poor molecules (694 molecules) were present in all seven HA samples but in none of the FA samples. In contrast, many oxygen-rich molecules (90 molecules) were present in all seven FA samples but in none of the HA samples. The more pronounced oxidised character (NOSC, O/C, Table A.12.) of FA matches with the larger solubility of these compounds in acids when compared with HA. On the other hand, the more pronounced presence of condensed aromatics in HA is consistent with their more hydrophobic character (Zherebker et al., 2019).

4.2. Quality changes across the reservoir

The results showed that the quality of sedimentary HS clearly changed along Itupararanga Reservoir. The upstream sites of the reservoir (locations P1 and P2) presented the highest C:N ratios (cf. Fig. 2 e), suggesting more pronounced contributions of land-plants as precursor material. This is supported by the lower FI values (cf. Fig. 2 c) and larger presence of aromatic C groups in FA samples from the upper reaches. These aromatic groups are related to lignin and condensed aromatic compounds from terrestrial sources (Sanderman et al., 2015). On the other hand, the sampling locations P3, P6 and P7 presented the lowest C:N values (around 10 for HA), thus suggesting greater algal contribution. This finding is also consistent with higher FI values and ^{13}C NMR results. Near-dam FA samples (particularly P5FA and P7FA) for example had more alkyl C, carbonyl C and N-alkyl/methoxyl C and lower amounts of carboxyl/amide C when compared to samples from the upper reaches of the reservoir. In addition, the near-dam samples had higher aliphaticity when compared to other FA samples. This can be observed in Fig. 4, where these samples (located on the right side of group I in Fig. 4 a) presented higher intensities (Fig. 4 b) for aliphaticity among all FA samples. These characteristics probably reflected the larger algal and microbial contribution of these samples (Derrien et al., 2017). Both FA and HA intensity weighted parameters AI_{mod} and DBE (Table A.12, Appendix A) also indicated that the near-dam sediment material is less aromatic than the upstream material. The increase of more aliphatic compounds in HA fraction at the dam (low AI_{mod} value, high intensities for molecules with $H/C > 1$ and $O/C < 0.5$) support this hypothesis. However, the predominant origin of HS from sediments across all reservoir was most likely terrestrial because FI values were below 1.4 in all sites (McKnight et al., 2001).

The larger presence of land-plant compounds in the upstream reaches contrasts with a recent investigation that found the upper reaches of the reservoir (P1 - P2) to have larger algal concentrations (higher chlorophyll-a levels) than the dam area (Melo et al., 2019). A possible explanation for that is the higher input of terrigenous-derived matter from the main inflow (generally the organic matter in rivers is mostly derived from allochthonous sources) into the upstream reaches of the reservoir (Park et al., 2009). Furthermore, fractions of terrestrial organic matter are more susceptible to gravitational settling and burial than in-lake matter (Guillemette et al., 2017). In fact, most of the particulate organic carbon in the reservoir was found to be internally produced (Bueno et al., 2020). Consequently, higher proportions of autochthonous organic matter may have been transported towards the dam.

Further differences between upper reaches and dam area were detected by β/α results: while upstream sites of the reservoir (P1 - P2) had larger proportions of older and more decomposed material with lower β/α values (cf. Fig. 2 a), samples from the dam area (P5 - P7) had higher content of fresh microbially derived matter (higher β/α). Wilson and Xenopoulos (2008) pointed out that this microbially-derived character may be related to the increased availability of nitrogen derived from agricultural lands to the microbial community. In fact, our self-organising maps showed that sampling sites (e.g. P6HA, group V and P6FA, group I, Fig. 4 a) under influence of higher proportions of agricultural/silviculture lands had higher β/α. This is confirmed by neurons with

higher intensities in the map of β/α. These correspond to neurons at equivalent positions that also had higher intensities in maps of agriculture and silviculture (Fig. 4 b). In addition, high total nitrogen concentrations recorded in waters of the Itupararanga Reservoir with values of 1.2 and 2.2 mg L^{-1} in surface and bottom waters were recorded in the dam area at site P6 (Melo et al., 2019). This supports the hypothesis of availability of nitrogen linked to OM with microbially-derived character (Wilson and Xenopoulos, 2008).

The $\delta^{13}C$ composition of sediments was nearly constant along the reservoir for most samples and indicated the predominance of C3 plants (Fig. 2 f). However, the enrichment of ^{13}C in the sediments collected at P5 and P6 may indicate an admixture of material from C4 plants. These plants may be derived for instance from agricultural activities in areas near these sampling sites. Corn and/or sugarcane (C4 plants) are possible contributors. These plants are common along Sorocaba River catchment (Smith et al., 2009).

The samples were relatively enriched in $\delta^{15}N$ that may reflect a mix of typical $\delta^{15}N$ signatures of plankton (+8‰), C3 land plants (+1‰) and soil organic matter (0 to +5‰), (Meyers and Ishiwatari, 1993; Finlay and Kendall, 2008). In addition, the decomposition process and microbial processing of the organic matter during the HS formation probably enriched the samples in ^{15}N due to losses of the isotopically lighter nitrogen (^{14}N, which generally reacts more easily) (See and Bronk, 2005; Liao et al., 2006; Craine et al., 2015). However, the isotopic values may also be a contribution of increased rates of mineralisation and nitrification triggered by conversion of forests to agricultural lands (Awiti et al., 2008). In fact, Salles et al. (2008) reported increasing deforestation rates in the catchment.

Regarding land use, the self-organising maps analysis indicated that the more pronounced presence of aromatic and terrestrial material in the upper reaches of the reservoir may be attributed to a larger proportion of grass and pasture lands and urban areas (Table A.14, Appendix A). This is confirmed by higher intensities of these variables at the same neuron (Fig. 4 b). This increase of terrestrial derived matter might be the result of conversion of forested areas to grass and pasture areas that may have led to enhanced leaching of soils. Consequently, the amount of terrestrial matter carried into the reservoir was supported (Salles et al., 2008; Melo et al., 2019). Forests probably also contributed to this material because they cover a larger proportion of the whole catchment (36.4%, Table A.14, Appendix A). A summary of all information extracted from all techniques and variables applied is presented in Table A.15 (Appendix A).

4.3. Further quality changes and biogeochemical processes

The increase of autochthonous material towards the dam was accompanied by a higher part of CHNO in the FA fraction as shown by the elevated N/C level (Table A.12, Appendix A) and inter sample ranking analysis (Fig. A.8, Appendix A). The FA fraction near the dam was more oxidised when compared to the upstream part. This may be explained by microbial or photochemical oxidation of dissolved or particulate organic material in flow direction before settling to the sediment. In fact, OM derived from allochthonous sources such as vascular plant-derived polyphenols (including lignin and tannins) and highly unsaturated and phenolic-derived compounds (probably present at upper reaches of the reservoir) are photoreactive (Kellerman et al., 2014; Wilske et al., 2020). The photodegradation of dissolved OM causes a decrease in aromatic compounds that are converted into more saturated and oxygenated compounds, which reflects in higher O/C ratios (Gonsior et al., 2009; Riedel et al., 2013). This increase in O/C ratios (Table A.12, Appendix A) and amounts of oxygen-rich compounds of FA (Fig. A.8, Appendix A) towards the dam supports the photochemical oxidation of OM across the reservoir. Near-dam samples P5FA, P6FA and P7FA showed many compounds with first to third (inter sample) ranks with van Krevelen coordinates H/C > 1 and O/C > 0.5. Such compounds were recently identified as photo products in a reservoir monitoring study (Herzsprung et al., 2020). For example, the compound $C_9H_{12}O_5$, which is a photo product, had the intensity rank 219 (inter sample rank 1) in PFA7 and rank 451 (inter sample rank 5) in PFA1. Such oxygen-rich and relative saturated compounds might be complexed to iron by carboxylic or phenolic moieties and finally settled to the sediment. In contrast, photo-degraded compounds like $C_{19}H_{22}O_7$, (PFA7: rank 1208; PFA1: rank 495; H/C 1.16; O/C 0.37) can be found at higher ratios in the near upstream samples, because their abundance is reduced in flow direction. This example would explain that light exposure and photochemical reactions are also responsible for the flocculation or the conversion (involving Fe as the catalyst) of allochthonous dissolved OM into particulate OM. This conversion is followed by sedimentation, reallocating OM from the water column to the sediments of the reservoir (Gao and Zepp, 1998; von Wachenfeldt et al., 2008). The presence of significant concentrations of dissolved Fe in surface waters (Melo et al. (2019) reported levels up to 485 μg L^{-1} at P1 and 517 μg L^{-1} at P2) from Itupararanga may contribute to the conversion of aromatic compounds. Several authors observed such photochemically induced changes and/or flocculation of dissolved OM in the presence of Fe after 21 to 72 h of sunlight exposure (Gao and Zepp, 1998; Gonsior et al., 2009). Since the residence time in Itupararanga reservoir is on average 250 days, OM has enough time to undergo photochemical reactions. As a consequence of all these processes, the amounts of autochthonous and photoresistant aliphatic compounds in sedimentary HS increased towards the dam area as the load of allochthonous components decreased via photodegradation and sedimentation (Kellerman et al., 2014).

Both fractions FA and HA are oxygen-poor and more aromatic in the upstream region. In the middle of the reservoir (P3, P5) especially the HA fraction was enriched in oxygen-rich and unsaturated compounds (Fig. A.9, Appendix A). The increase of oxygen-rich compounds in HA samples from the middle of the reservoir may also be related to photodegradation. However, near-dam HA samples (P6 - P7) were poorer in oxygen (which would be produced from photooxidation). The ^{13}C NMR data indicated that the amount of aromatic C in HA did not change much along the reservoir (Fig. A.5, Appendix A). This indicates that the photooxidation may be more important to FA, possibly because of their higher solubility in water at lower pH (the FA molecules would stay longer in the water column and would be more susceptible to resuspension during seasonal mixing than HA). The indication that HA turned more aliphatic at near-dam sites by FT-ICR-MS contrast with ^{13}C NMR results. This may be linked to possible loss of some HA compounds during SPE, which is poor in extracting high molecular weight components (Hawkes et al., 2019). In addition, higher molecular weight fractions (especially the more aromatic and coloured) are more difficult to ionise via ESI (Reemtsma and These, 2003; These and Reemtsma, 2003). Consequently, the detected differences between upstream and near-dam sites by FT-ICR-MS were too small to be resolved via NMR and corresponded just to extractable and ionisable aromatic molecules.

The oxidation of aromatic compounds may also be related either to a reduced amount of aromatic OM reaching dam-area or via interactions between Fe and aromatic OM. These Fe-OM interactions generally occur under anaerobic conditions where Fe (III) is an important electron acceptor for oxidation of aromatic HS (Lovley et al., 1989, 1996). Microorganisms can further enhance this process (Lovley et al., 1989; Roden et al., 2010; Kulkarni et al., 2018). Indeed, the reservoir has a seasonal stratification, where high amounts of Fe in anoxic and reducing waters was recorded

at its bottom waters (2370 μg L^{-1} at P4 and 672 μg L^{-1} at P6) from the intermediate and dam area (P4 - P7) (Melo et al., 2019). Therefore, loss of aromatic compounds may also be derived from reduction of Fe in deeper waters from Itupararanga Reservoir. The mobility of aromatic compounds from anoxic pore waters and surface sediments may also be affected by retention in redox interfaces between sediments and water column via co-precipitation with Fe(III), reducing the amount of these compounds in sediments (Riedel et al., 2013).

4.4. Self-organising maps and principal component analysis

The PCA results (Fig. 5) showed that the first (PC1) and the second (PC2) principal components explained 58.47% of the total variance in the sedimentary HS. The biplot indicated the presence of seven groups (i to vii, Fig. 5) that reflected OM quality between FA and HA and upstream and near-dam sites, similar to the self-organising maps. The first component for instance explained most of data variability (33.21%) and was responsible for the discrimination between HA (groups i to iii) and FA (groups iv to vii). The variables CHNO, CHNOS, aromaticity and aromatic carbon were the most positively correlated to HA. Similar interpretations were observed in the self-organising maps (cf. Section 3.5). In summary, both techniques can be efficiently used to cluster data and interpret results. However, self-organising maps have several advantages over PCA (Richardson et al., 2003; Brereton, 2012), including:

- better visualisation capabilities;
- space is more efficiently used in self-organising maps. In contrast, groups in PC plots can be tightly clustered or overlapped, leaving large empty areas. Moreover, the PC plots can be crowded, becoming hard to distinguish samples and/or variables;
- it is not necessary to choose which PCs have to be used for visualisation (sometimes it is necessary to use more than two components to get more insights);
- self-organising maps are more effective to cope with noisy and missing data;
- self-organising maps have more possibilities for graphical representation.

5. Conclusions

Our multi-proxy approach in combination with self-organising maps pointed out significant differences between sedimentary FA and HA from the dam zone when compared to upper reaches of the Itupararanga Reservoir. In summary, samples from areas in the upstream reaches of the reservoir were older, more decomposed and had a larger contribution of land plants as precursor material. Furthermore, these samples had larger presence of oxygen-poor compounds in FA and HA and more unsaturated compounds (HA) and aromatic, carboxyl and amide C groups. On the other hand, samples (FA) from the dam area were fresher and presented a more pronounced contribution of autochthonous phytoplankton and microbially-derived matter. With this, a larger presence of alkyl and carbonyl C groups were detected in FA from dam area. They also had a more pronounced presence of oxygen-rich (FA) compounds. In contrast, HA were poorer in oxygen when compared to FA. These differences between upstream and dam area indicated that in-lake processes such as photooxidation of aromatic compounds may have affected HS quality towards the dam area.

The combination of different complementary techniques provided valuable information about the nature of FA and HA in Itupararanga Reservoir. The self-organising maps supported the interpretation of the results and helped to find relationships between samples and variables. Furthermore, the analyses indicated that FA were better than HA samples for finding inter-site differences. Such a multi-proxy approach could be transferred to other reservoirs worldwide for understanding transformations and processes involving sedimentary OM in these environments.

Declaration of Competing Interest

The authors declare that they have no known competing financial interests or personal relationships that could have appeared to influence the work reported in this paper.

Acknowledgments

This investigation was supported by Coordenação de Aperfeiçoamento de Pessoal de Nível Superior (CAPES) and Deutscher

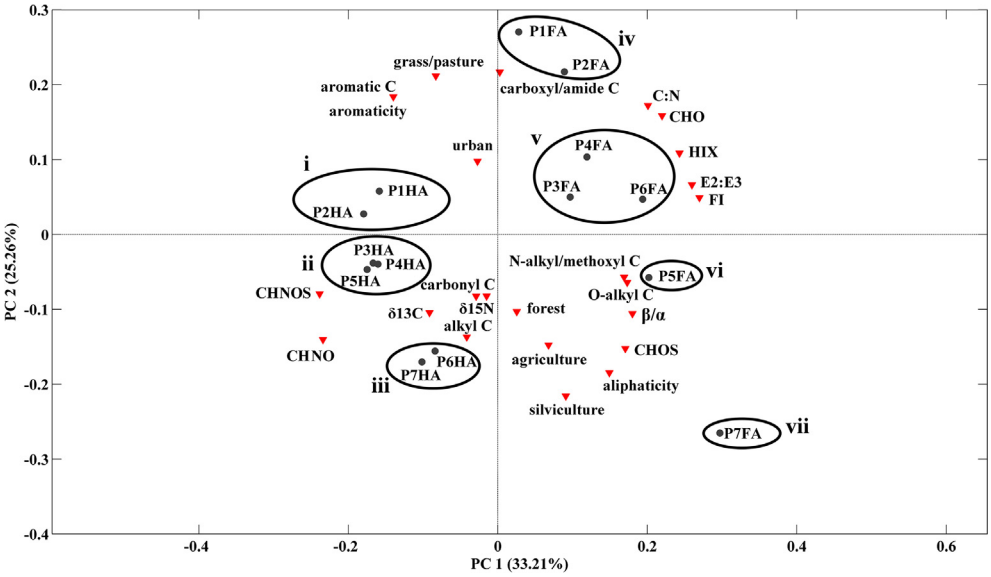

Fig. 5. Principal component analysis (biplot of the first two principal components, PC1 versus PC2) for sedimentary fulvic (FA) and humic acids (HA). Circles represent fulvic or humic acid samples from seven sampling sites in Itupararanga Reservoir. Inverted triangles represent the variables.

Akademischer Austauschdienst (DAAD) through the project "Organic carbon cycling in water reservoirs – ORCWAR" (DAAD-ID 57414997; CAPES 99999.008107/2015-07, 88887.141964/2017-00 and 88887.303733/2018-00). We also acknowledge the financial assistance of Fundação de Amparo à Pesquisa do Estado de São Paulo (FAPESP, grant number 18/20326-1) and Conselho Nacional de Desenvolvimento Científico e Tecnológico (CNPq, grant number 158227/2018-2). The authors thank Christian Hanke, Jan Kaesler and Michael Herzog for help and assistance during field trips and laboratory analyses. We also thank the Otto Von Guericke Universität Magdeburg for the analyses of ^{13}C NMR, especially Ms. Liane Hilfert for her assistance. The authors are grateful for using the analytical facilities of the Centre for Chemical Microscopy (ProVIS) at the Helmholtz Centre for Environmental Research, Leipzig which is supported by the European Regional Development Funds (EFRE - Europe funds Saxony) and the Helmholtz Association. We also thank the anonymous reviewers for their many constructive comments and suggestions that contributed to improve this manuscript. The authors acknowledge the efforts of the associate editor, Marcus Elvert, for his handling of the manuscript.

Data Availability

Research data associated with this article can be accessed at https://doi.org/10.17632/r86jr7x6dz.1.

Appendix A. Supplementary material

Supplementary data to this article can be found online at https://doi.org/10.1016/j.orggeochem.2020.104165.

Associate Editor—**Marcus Elvert**

References

Alhoniemi, E., Himberg, J., Parhankangas, J., Vesanto, J., 2000. SOM Toolbox.
Asan, U., Ercan, S., 2012. An introduction to self-organizing maps. In: Kahraman, C. (Ed.), Computational Intelligence Systems in Industrial Engineering: With Recent Theory and Applications. Atlantis Press, Paris, pp. 295–315.
Awiti, A.O., Walsh, M.G., Kinyamario, J., 2008. Dynamics of topsoil carbon and nitrogen along a tropical forest–cropland chronosequence: evidence from stable isotope analysis and spectroscopy. Agriculture, Ecosystems & Environment 127, 265–272.
Brereton, R.G., 2012. Self organising maps for visualising and modelling. Chemistry Central Journal 6, S1.
Bueno, C.d.C., Frascareli, D., Gontijo, E.S.J., van Geldern, R., Rosa, A.H., Friese, K., Barth, J.A.C., 2020. Dominance of in situ produced particulate organic carbon in a subtropical reservoir inferred from carbon stable isotopes. Scientific Reports 10, 13187.
Chen, M., Hur, J., 2015. Pre-treatments, characteristics, and biogeochemical dynamics of dissolved organic matter in sediments: a review. Water Research 79, 10–25.
Çinar, O., Merdun, H., 2009. Application of an unsupervised artificial neural network technique to multivariant surface water quality data. Ecological Research 24, 163–173.
Conte, P., Piccolo, A., van Lagen, B., Buurman, P., Hemminga, M.A., 2002. Elemental quantitation of natural organic matter by CPMAS 13C NMR spectroscopy. Solid State Nuclear Magnetic Resononance 21, 158–170.
Craig, H., 1957. Isotopic standards for carbon and oxygen and correction factors for mass-spectrometric analysis of carbon dioxide. Geochimica et Cosmochimica Acta 12, 133–149.
Craine, J.M., Brookshire, E.N.J., Cramer, M.D., Hasselquist, N.J., Koba, K., Marin-Spiotta, E., Wang, L., 2015. Ecological interpretations of nitrogen isotope ratios of terrestrial plants and soils. Plant and Soil 396, 1–26.
da Silva, G.A., Augusto, F., Poppi, R.J., 2008. Exploratory analysis of the volatile profile of beers by HS–SPME–GC. Food Chemistry 111, 1057–1063.
Dadi, T., Harir, M., Hertkorn, N., Koschorreck, M., Schmitt-Kopplin, P., Herzsprung, P., 2017. Redox conditions affect dissolved organic carbon quality in stratified freshwaters. Environmental Science & Technology 51, 13705–13713.
de la Rosa, J.M., González-Pérez, J.A., González-Vila, F.J., Knicker, H., Araújo, M.F., 2011. Molecular composition of sedimentary humic acids from South West Iberian Peninsula: a multi-proxy approach. Organic Geochemistry 42, 791–802.
de Miranda, E.E., 2005. Brasil em Relevo. Empresa Brasileira de Pesquisa Agropecuária - Embrapa, Campinas.
Dean, W.E., 1974. Determination of carbonate and organic matter in calcareous sediments and sedimentary rocks by loss on ignition; comparison with other methods. Journal of Sedimentary Research 44, 242–248.
Derrien, M., Lee, Y.K., Park, J.-E., Li, P., Chen, M., Lee, S.H., Lee, S.H., Lee, J.-B., Hur, J., 2017. Spectroscopic and molecular characterization of humic substances (HS) from soils and sediments in a watershed: comparative study of HS chemical fractions and the origins. Environmetnal Science and Pollution Research 24, 16933–16945.
Derrien, M., Lee, Y.K., Shin, K.-H., Hur, J., 2018. Comparing discrimination capabilities of fluorescence spectroscopy versus FT-ICR-MS for sources and hydrophobicity of sediment organic matter. Environmetnal Science and Pollution Research 25, 1892–1902.
Dittmar, T., Koch, B., Hertkorn, N., Kattner, G., 2008. A simple and efficient method for the solid-phase extraction of dissolved organic matter (SPE-DOM) from seawater. Limnology and Oceanography: Methods 6, 230–235.
Ejarque-Gonzalez, E., Butturini, A., 2014. Self-organising maps and correlation analysis as a tool to explore patterns in excitation-emission matrix data sets and to discriminate dissolved organic matter fluorescence components. PLOS ONE 9, e99618.
Elkins, K.M., Nelson, D.J., 2002. Spectroscopic approaches to the study of the interaction of aluminum with humic substances. Coordination Chemistry Reviews 228, 205–225.
Finlay, J.C., Kendall, C., 2008. Stable isotope tracing of temporal and spatial variability in organic matter sources to freshwater ecosystems. Stable Isotopes in Ecology and Environmental Science, 283–333.
Flerus, R., Lechtenfeld, O.J., Koch, B.P., McCallister, S.L., Schmitt-Kopplin, P., Benner, R., Kaiser, K., Kattner, G., 2012. A molecular perspective on the ageing of marine dissolved organic matter. Biogeosciences 9, 1935–1955.
Frascareli, D., Beghelli, F.G.d.S., Silva, S.C.d., Carlos, V.M., 2015. Heterogeneidade espacial e temporal de variáveis limnológicas no reservatório de Itupararanga associadas com o uso do solo na Bacia do Alto Sorocaba-SP. Revista Ambiente & Água 10, 770–781.
Frascareli, D., Cardoso-Silva, S., de Oliveira Soares-Silva Mizael, J., Rosa, A.H., Pompeo, M.L.M., Lopez-Doval, J.C., Moschini-Carlos, V., 2018. Spatial distribution, bioavailability, and toxicity of metals in surface sediments of tropical reservoirs, Brazil. Environmental Monitoring and Assessment 190, 199.
Gao, H., Zepp, R.G., 1998. Factors influencing photoreactions of dissolved organic matter in a Coastal River of the Southeastern United States. Environmental Science & Technology 32, 2940–2946.
Garcia, J.S., Da Silva, G.A., Arruda, M.A.Z., Poppi, R.J., 2007. Application of Kohonen neural network to exploratory analyses of synchroton radiation x-ray fluorescence measurements of sunflower metalloproteins. X-Ray Spectrometry 36, 122–129.
Gonsior, M., Peake, B.M., Cooper, W.T., Podgorski, D., D'Andrilli, J., Cooper, W.J., 2009. Photochemically induced changes in dissolved organic matter identified by ultrahigh resolution Fourier transform ion cyclotron resonance mass spectrometry. Environmental Science & Technology 43, 698–703.
Guillemette, F., von Wachenfeldt, E., Kothawala, D.N., Bastviken, D., Tranvik, L.J., 2017. Preferential sequestration of terrestrial organic matter in boreal lake sediments. J. Geophysical Research: Biogeosciences 122, 863–874.
Hansen, A.M., Kraus, T.E.C., Pellerin, B.A., Fleck, J.A., Downing, B.D., Bergamaschi, B. A., 2016. Optical properties of dissolved organic matter (DOM): effects of biological and photolytic degradation. Limnology and Oceanography 61, 1015–1032.
Hawkes, J.A., Sjöberg, P.J.R., Bergquist, J., Tranvik, L.J., 2019. Complexity of dissolved organic matter in the molecular size dimension: insights from coupled size exclusion chromatography electrospray ionisation mass spectrometry. Faraday Discussions 218, 52–71.
Helms, J.R., Stubbins, A., Ritchie, J.D., Minor, E.C., Kieber, D.J., Mopper, K., 2008. Absorption spectral slopes and slope ratios as indicators of molecular weight, source, and photobleaching of chromophoric dissolved organic matter. Limnology and Oceanography 53, 955–969.
Hertkorn, N., Harir, M., Koch, B.P., Michalke, B., Schmitt-Kopplin, P., 2013. High-field NMR spectroscopy and FTICR mass spectrometry: powerful discovery tools for the molecular level characterization of marine dissolved organic matter. Biogeosciences 10, 1583–1624.
Herzsprung, P., Hertkorn, N., von Tümpling, W., Harir, M., Friese, K., Schmitt-Kopplin, P., 2016. Molecular formula assignment for dissolved organic matter (DOM) using high-field FT-ICR-MS: chemical perspective and validation of sulphur-rich organic components (CHOS) in pit lake samples. Analytical and Bioanalytical Chemistry 408, 2461–2469.
Herzsprung, P., Osterloh, K., von Tümpling, W., Harir, M., Hertkorn, N., Schmitt-Kopplin, P., Meissner, R., Bernsdorf, S., Friese, K., 2017a. Differences in DOM of rewetted and natural peatlands – results from high-field FT-ICR-MS and bulk optical parameters. Science of The Total Environment 586, 770–781.
Herzsprung, P., von Tümpling, W., Hertkorn, N., Harir, M., Büttner, O., Bravidor, J., Friese, K., Schmitt-Kopplin, P., 2012. Variations of DOM quality in inflows of a drinking water reservoir: linking of van Krevelen diagrams with EEMF spectra by rank correlation. Environmental Science & Technology 46, 5511–5518.

Herzsprung, P., von Tümpling, W., Wendt-Potthoff, K., Hertkorn, N., Harir, M., Schmitt-Kopplin, P., Friese, K., 2017b. High field FT-ICR mass spectrometry data sets enlighten qualitative DOM alteration in lake sediment porewater profiles. Organic Geochemistry 108, 51–60.
Herzsprung, P., Wentzky, V., Kamjunke, N., von Tümpling, W., Wilske, C., Friese, K., Boehrer, B., Reemtsma, T., Rinke, K., Lechtenfeld, O.J., 2020. Improved understanding of dissolved organic matter processing in freshwater using complementary experimental and machine learning approaches. Environmental Science & Technology 54, 13556–13565.
Hur, J., Kim, G., 2009. Comparison of the heterogeneity within bulk sediment humic substances from a stream and reservoir via selected operational descriptors. Chemosphere 75, 483–490.
Hur, J., Lee, B.-M., Shin, K.-H., 2014. Spectroscopic characterization of dissolved organic matter isolates from sediments and the association with phenanthrene binding affinity. Chemosphere 111, 450–457.
Kellerman, A.M., Dittmar, T., Kothawala, D.N., Tranvik, L.J., 2014. Chemodiversity of dissolved organic matter in lakes driven by climate and hydrology. Nature Communications 5, 3804.
Knicker, H., Lüdemann, H.D., 1995. N-15 and C-13 CPMAS and solution NMR studies of N-15 enriched plant material during 600 days of microbial degradation. Organic Geochemistry 23, 329–341.
Koch, B.P., Dittmar, T., 2006. From mass to structure: an aromaticity index for high-resolution mass data of natural organic matter. Rapid Communications in Mass Spectrometry 20, 926–932.
Koch, B.P., Kattner, G., Witt, M., Passow, U., 2014. Molecular insights into the microbial formation of marine dissolved organic matter: recalcitrant or labile? Biogeosciences 11, 4173–4190.
Kulkarni, H.V., Mladenov, N., McKnight, D.M., Zheng, Y., Kirk, M.F., Nemergut, D.R., 2018. Dissolved fulvic acids from a high arsenic aquifer shuttle electrons to enhance microbial iron reduction. Science of The Total Environment 615, 1390–1395.
LaRowe, D.E., Van Cappellen, P., 2011. Degradation of natural organic matter: a thermodynamic analysis. Geochimica et Cosmochimica Acta 75, 2030–2042.
Li, Z., Xu, X., Ji, M., Wang, G., Han, R., Ma, J., Yan, X., Liu, J., 2018. Estimating sedimentary organic matter sources by multi-combined proxies for spatial heterogeneity in a large and shallow eutrophic lake. Journal of Environmental Management 224, 147–155.
Liao, J.D., Boutton, T.W., Jastrow, J.D., 2006. Organic matter turnover in soil physical fractions following woody plant invasion of grassland: Evidence from natural 13C and 15N. Soil Biology and Biochemistry 38, 3197–3210.
Lovley, D.R., Baedecker, M.J., Lonergan, D.J., Cozzarelli, I.M., Phillips, E.J.P., Siegel, D.I., 1989. Oxidation of aromatic contaminants coupled to microbial iron reduction. Nature 339, 297–300.
Lovley, D.R., Coates, J.D., Blunt-Harris, E.L., Phillips, E.J.P., Woodward, J.C., 1996. Humic substances as electron acceptors for microbial respiration. Nature 382, 445–448.
McDonald, S., Bishop, A.G., Prenzler, P.D., Robards, K., 2004. Analytical chemistry of freshwater humic substances. Analytica Chimica Acta 527, 105–124.
McKnight, D.M., Boyer, E.W., Westerhoff, P.K., Doran, P.T., Kulbe, T., Andersen, D.T., 2001. Spectrofluorometric characterization of dissolved organic matter for indication of precursor organic material and aromaticity. Limnology and Oceanography 46, 38–48.
Melendez-Perez, J.J., Martínez-Mejía, M.J., Awan, A.T., Fadini, P.S., Mozeto, A.A., Eberlin, M.N., 2016. Characterization and comparison of riverine, lacustrine, marine and estuarine dissolved organic matter by ultra-high resolution and accuracy Fourier transform mass spectrometry. Organic Geochemistry 101, 99–107.
Melo, D.S., Gontijo, E.S.J., Frascareli, D., Simonetti, V.C., Machado, L.S., Barth, J.A.C., Moschini-Carlos, V., Pompêo, M.L., Rosa, A.H., Friese, K., 2019. Self-organizing maps for evaluation of biogeochemical processes and temporal variations in water quality of subtropical reservoirs. Water Resources Research 55, 10268–10281.
Meyers, P.A., 1994. Preservation of elemental and isotopic source identification of sedimentary organic matter. Chemical Geology 114, 289–302.
Meyers, P.A., Ishiwatari, R., 1993. Lacustrine organic geochemistry—an overview of indicators of organic matter sources and diagenesis in lake sediments. Organic Geochemistry 20, 867–900.
Minor, E.C., Swenson, M.M., Mattson, B.M., Oyler, A.R., 2014. Structural characterization of dissolved organic matter: a review of current techniques for isolation and analysis. Environmental Science: Processes & Impacts 16, 2064–2079.
Nguyen, L.M., 1999. Phosphate incorporation and transformation in surface sediments of a sewage-impacted wetland as influenced by sediment sites, sediment pH and added phosphate concentration. Ecological Engineering 14, 139–155.
Ohno, T., 2002. Fluorescence inner-filtering correction for determining the humification index of dissolved organic matter. Environmental Science & Technology 36, 742–746.
Park, H.-K., Byeon, M.-S., Shin, Y.-N., Jung, D.-I., 2009. Sources and spatial and temporal characteristics of organic carbon in two large reservoirs with contrasting hydrologic characteristics. Water Resources Research 45.
Parlanti, E., Wörz, K., Geoffroy, L., Lamotte, M., 2000. Dissolved organic matter fluorescence spectroscopy as a tool to estimate biological activity in a coastal zone submitted to anthropogenic inputs. Organic Geochemistry 31, 1765–1781.
Pedrazzi, F.J.d.M., Conceição, F.T.d., Sardinha, D.d.S., Moschini-Carlos, V., Pompêo, M., 2013. Spatial and Temporal Quality of Water in the Itupararanga Reservoir, Alto Sorocaba Basin (SP), Brazil. Journal of Water Resource and Protection 5, 64–71.
Raeke, J., Lechtenfeld, O.J., Wagner, M., Herzsprung, P., Reemtsma, T., 2016. Selectivity of solid phase extraction of freshwater dissolved organic matter and its effect on ultrahigh resolution mass spectra. Environmental Science: Processes & Impacts 18, 918–927.
Raposo, J.C., Villanueva, U., Olivares, M., Madariaga, J.M., 2016. Determination of humic substances in sediments by focused ultrasound extraction and ultraviolet visible spectroscopy. Microchemical Journal 128, 26–33.
Reemtsma, T., These, A., 2003. On-line coupling of size exclusion chromatography with electrospray ionization-tandem mass spectrometry for the analysis of aquatic fulvic and humic acids. Analytical Chemistry 75, 1500–1507.
Ribeiro, A.R., Biagioni, R.C., Smith, W.S., 2014. Estudo da dieta natural da ictiofauna de um reservatório centenário, São Paulo, Brasil. Iheringia. Série Zoologia 104, 404–412.
Richardson, A.J., Risien, C., Shillington, F.A., 2003. Using self-organizing maps to identify patterns in satellite imagery. Progress in Oceanography 59, 223–239.
Riedel, T., Zak, D., Biester, H., Dittmar, T., 2013. Iron traps terrestrially derived dissolved organic matter at redox interfaces. Proceedings of the National Academy of Sciences 110, 10101–10105.
Roden, E.E., Kappler, A., Bauer, I., Jiang, J., Paul, A., Stoesser, R., Konishi, H., Xu, H., 2010. Extracellular electron transfer through microbial reduction of solid-phase humic substances. Nature Geoscience 3, 417–421.
Rodrigues, E.H.C., Vicentin, A.M., Machado, L.d.S., Pompêo, M.L.M., Carlos, V.M., 2019. Phytoplankton, Trophic State and Ecological Potential in reservoirs in the State of São Paulo, Brazil. Revista Ambiente & Água 14.
Rodríguez-Murillo, J.C., Almendros, G., Knicker, H., 2011. Wetland soil organic matter composition in a Mediterranean semiarid wetland (Las Tablas de Daimiel, Central Spain): Insight into different carbon sequestration pathways. Organic Geochemistry 42, 762–773.
Rosa, A.H., Silva, Â.A.M.J., Melo, C.d.A., Moschini, V., Carlos, M., Guandique, E.G., Fraceto, L.F., Lourenço, R.W., 2015. Diagnóstico ambiental e avaliação de uso e ocupação do solo visando a sustentabilidade da represa de Itupararanga, importante área da bacia do médio Tietê, Ecologia de reservatórios e interfaces. Instituto de Biociências da Universidade de São Paulo, São Paulo, pp. 213–231.
Salles, M.D.H., Conceição, F.T., Angelucci, V.A., Sia, R., Pedrazzi, F.J.M., Carra, T.A., Monteiro, G.F., Sardinha, D.d.S., Navarro, G.R.B., 2008. Simplified environmental impact assessment in Alto Sorocaba Basin (SP). Revista de estudos ambientais 10, 6–20.
Sanderman, J., Krull, E., Kuhn, T., Hancock, G., McGowan, J., Maddern, T., Fallon, S., Steven, A., 2015. Deciphering sedimentary organic matter sources: Insights from radiocarbon measurements and NMR spectroscopy. Limnology and Oceanography 60, 739–753.
See, J.H., Bronk, D.A., 2005. Changes in C: N ratios and chemical structures of estuarine humic substances during aging. Marine Chemistry 97, 334–346.
Shen, Z., Hou, X., Li, W., Aini, G., Chen, L., Gong, Y., 2015. Impact of landscape pattern at multiple spatial scales on water quality: a case study in a typical urbanised watershed in China. Ecological Indicators 48, 417–427.
Smith, W., Petrere Jr., M., Barrella, W., 2009. The fish community of the Sorocaba River Basin in different habitats (State of São Paulo, Brazil). Brazilian Journal of Biology 69, 1015–1025.
Swift, R.S., 1996. Organic matter characterization. In: Sparks, D.L., Page, A.L., Helmke, P.A., Loeppert, R.H. (Eds.), Methods of Soil Analysis Part 3—Chemical Methods. Soil Science Society of America, American Society of Agronomy, Madison, WI, pp. 1011–1069.
These, A., Reemtsma, T., 2003. Limitations of electrospray ionization of fulvic and humic acids as visible from size exclusion chromatography with organic carbon and mass spectrometric detection. Analytical Chemistry 75, 6275–6281.
Torres, I.C., Inglett, P.W., Brenner, M., Kenney, W.F., Ramesh Reddy, K., 2012. Stable isotope (δ13C and δ15N) values of sediment organic matter in subtropical lakes of different trophic status. Journal of Paleolimnology 47, 693–706.
Valle, J., Gonsior, M., Harir, M., Enrich-Prast, A., Schmitt-Kopplin, P., Bastviken, D., Conrad, R., Hertkorn, N., 2018. Extensive processing of sediment pore water dissolved organic matter during anoxic incubation as observed by high-field mass spectrometry (FTICR-MS). Water Research 129, 252–263.
von Wachenfeldt, E., Sobek, S., Bastviken, D., Tranvik, L.J., 2008. Linking allochthonous dissolved organic matter and boreal lake sediment carbon sequestration: the role of light-mediated flocculation. Limnology and Oceanography 53, 2416–2426.
Wilske, C., Herzsprung, P., Lechtenfeld, O.J., Kamjunke, N., von Tümpling, W., 2020. Photochemically induced changes of dissolved organic matter in a humic-rich and forested stream. Water 12, 331.
Wilson, H.F., Xenopoulos, M.A., 2008. Effects of agricultural land use on the composition of fluvial dissolved organic matter. Nature Geoscience 2, 37.
Wolfe, A.P., Kaushal, S.S., Fulton, J.R., McKnight, D.M., 2002. Spectrofluorescence of sediment humic substances and historical changes of lacustrine organic matter provenance in response to atmospheric nutrient enrichment. Environmetnal Science & Technology 36, 3217–3223.
Yang, X., Meng, L., Meng, F., 2019. Combination of self-organizing map and parallel factor analysis to characterize the evolution of fluorescent dissolved organic matter in a full-scale landfill leachate treatment plant. Science of The Total Environment 654, 1187–1195.
Zherebker, A., Podgorski, D.C., Kholodov, V.A., Orlov, A.A., Yaroslavtseva, N.V., Kharybin, O., Kholodov, A., Spector, V., Spencer, R.G.M., Nikolaev, E., Perminova, I.V., 2019. The molecular composition of humic substances isolated from yedoma permafrost and alas cores in the eastern Siberian arctic as measured by

ultrahigh resolution mass spectrometry. Journal of Geophysical Research: Biogeosciences 124, 2432–2445.
Zherebker, A.Y., Kostyukevich, Y.I., Kononikhin, A.S., Nikolaev, E.N., Perminova, I.V., 2016. Molecular compositions of humic acids extracted from leonardite and lignite as determined by Fourier transform ion cyclotron resonance mass spectrometry. Mendeleev Communications 26, 446–448.
Zorzal-Almeida, S., Salim, A., Andrade, M.R.M., Nascimento, M.d.N., Bini, L.M., Bicudo, D.C., 2018. Effects of land use and spatial processes in water and surface sediment of tropical reservoirs at local and regional scales. Science of The Total Environment 644, 237–246.